



Semi-rigid Composite Beam-to-column Joints for Cold-formed Steel Frames: Experimental and Numerical Study

Faisal Amsyar¹ · Cher Siang Tan² · Arizu Sulaiman² · Shahrin Mohammad³

Received: 12 August 2022 / Accepted: 11 April 2023 / Published online: 20 April 2023
© Korean Society of Steel Construction 2023

Abstract

An experimental and numerical study was performed to evaluate the structural behaviour of the semi-rigid composite cold-formed steel beam-to-column joints, in terms of its strength and stiffness. Five composite joints were subjected to different diameters of rebar (8 mm and 10 mm) with varying types of reinforcing bar (high-strength rebar, mild-strength rebar and high-strength steel wire mesh) and different thicknesses of concrete slab (100 mm and 125 mm). Isolated joint tests were dispensed to all specimens by using 100 kN capacity of hydraulic jack to induce axial point load. Non-linear finite element models were developed by using ABAQUS software for the joint configurations. A 3-D stress option with an eight-node linear brick element and no hourglass controls (C3D8) was proposed to simulate all steel and concrete components as it provided well analysis prediction with further simulation beyond ultimate load-bearing capacity. Good correlation was observed from comparison of both experimental and numerical results with strength ratios that ranged from 0.92 to 0.98. Ultimate strength was obtained by increasing the diameter of steel reinforcement, thickness of concrete slab and using high-strength steel reinforcing bar instead of mild-steel reinforcing bar and high-strength steel wire mesh.

Keywords Semi-rigid joint · Cold-formed steel lipped-channel section · Composite joint · Moment resistance · Initial stiffness · Finite element analysis

1 Introduction

The use of lightweight cold-formed members as a main structure in the construction of steel framing has increased and become widespread since it is one of the foremost exciting developments in structural steelwork to substitute other materials like hot-rolled steel (HRS) and timber. Earlier, between the year of 1850 and 1900, composite steel structure was introduced to the construction field and recent research on it had been well-developed and expended over the years. Since the composite structure was formed by integrating concrete slab into the steel structure, a composite action was created between the components, making the embedded reinforcing bars contributed most of the resisting strength and stiffness of the connection. A review by Amsyar et al. (2018) stated that the majority of the investigations in the past 20 years on composite CFS structures indicated that composite concrete-steel joint performed with higher load-bearing capacity, moment resistance and rotational stiffness as compared to the non-composite joint structures. The implementation of composite construction during these recent years was to reinforce the performance of partial

✉ Faisal Amsyar
famsyar2@graduate.utm.my

Cher Siang Tan
tcsiang@utm.my

Arizu Sulaiman
arizu@utm.my

Shahrin Mohammad
shahrin@utm.my

¹ School of Civil Engineering, Faculty of Engineering, Universiti Teknologi Malaysia, UTM Johor Bahru, 81310 Johor Bahru, Johor, Malaysia

² Department of Structure and Materials, School of Civil Engineering, Faculty of Engineering, Universiti Teknologi Malaysia, UTM Johor Bahru, 81310 Johor Bahru, Johor, Malaysia

³ Chancellery Strategic Management Office, Universiti Teknologi Malaysia, UTM Johor Bahru, 81310 Johor Bahru, Johor, Malaysia

strength connection as the combination of steel beams and concrete slab to resist load effects, which allowed utilisation of a high bending capacity through the durability of steel and compressive strength of concrete (Ozturk et al., 2019).

The term of partial strength and semi-rigid connection, as indicated in Eurocode 3, can be fulfilled if and only if the steel connection is having a moment resistance of joint smaller than the moment capacity of the connected members. Plenty of new configurations for the laboratory investigation and computational modelling were carried out by researchers to evaluate the structural and mechanical performance of steel–concrete composite structures, especially to the composite beams and beam-to-column joints (Hsu et al., 2014; Katwal et al., 2018; Lacki et al., 2019; Luo et al., 2012; Qiao et al., 2020; Zhao et al., 2012). Fahmy et al. (2020) proposed two different types of gusset plate in the study so as to analyse the structural behaviour of composite CFS connections and concluded that the ultimate load-bearing capacity was significantly improved by 72% when trapezoidal connector was used. Aminuddin et al. (2017) proved that plate connection was extremely ductile and might be categorised as pin connection through a physical test of full-scale isolated joint test on the beam-to-column of CFS joints. Hsu et al. (2014) proposed the use the transverse reinforcement in concrete slab with installation of bent rib (modified) of shear connector to the composite connections. Saggaff et al. (2017) through a laboratory study indicated that by using larger diameter of bolted shear connector it seemed to exhibit a much better performance and yielded higher load-bearing capacity and moment resistance for the composite connection. Although many research works were conducted experimentally, so as to ascertain the actual characteristics and performance of the composite steel connection, limited investigations on the non-linear behaviour were discovered because the physical tests were expensive and time-consuming. Concurring with Amsyar et al. (2021), who practised computational modelling by using a simulation software, the study was able to explore deeply into the corresponding variables, parametric studies and potential failure mechanisms to the composite CFS structures as the basic laboratory method was typical and cost-consuming. The non-linear finite elements method seemed to be an alternative and attractive tool to explore more into the massive scale of variables and potential failure modes that might occur to the composite CFS connection. According to Foraboschi (2020), modern structural engineering activity (including the research work) is based on an extensive use of the Finite Element (FE) method, which not only simplifies the work of the engineer but also allows bold structures to be designed, analyzed and constructed.

By considering non-linearities material, appropriate element types and adequate boundary conditions in the computational modelling, Kim et al. (2007) and Fu et al. (2008)

agreed that good correlation between both physical and numerical analyses could be achieved and well in predicting the ultimate strength of bolted moment joints in cold-formed steel structures. By adopting element type of C3D20R, 20-node quadratic brick meshing to simulate CFS top-seat flange cleat connection in light steel framing, Tan et al. (2013) revealed that similar failure modes were observed from the comparison of FEM models and physical experimental testing results; by having differences of initial stiffness and moment resistance up to 7% and 9%, respectively. Non-linear properties of materials and geometric analyses were administered by using ABAQUS (version 6.14) finite element package to analyse the stiffness and strength performance of top-seat flange-cleat connection for CFS double-channel sections, Huei et al. (2012) and Lee et al. (2013) discovered that differences of about 35% and 50% were shown, respectively, from the comparisons of moment-rotation relation between both numerical and laboratory data for the strength and rotational stiffness behaviour. Both agreed that about 18%–65% differences of capacity behaviour and 1%–153% differences of stiffness behaviour were recorded between FE models and analytical calculation (Huei et al., 2012; Lee et al., 2013). Firdaus et al. (2017) in a study of numerical modelling on the composite beam-to-column joint of CFS section had summarised that a good and promising agreement was perfectly achieved between FE and theoretical analyses.

From all of the review and discussions, it can be summarized that there is some sort of improvement that could be done to the limitation from previous studies. Therefore, this study is performing a clear framework and proposing some sort of parametric studies in order to overcome the limited scope of work that been conducted by previous researchers. The objective of this paper is to check on the joint behaviour of semi-rigid composite CFS connection. By employing a general-purpose finite element package ABAQUS Version 6.14, a three-dimensional (3-D) finite element model was proposed in this study. The study was conducted to verify the modelling approach and validate with the experimental results to obtain general characteristics of a full-scale composite CFS joint.

2 Experimental Programme

2.1 Test Specimens

To prepare the full-scale composite CFS beam-to-column joint specimen, each of the involved components such as CFS beam and column sections, hot-rolled steel (HRS) gusset plate, CFS shear connectors, thin-plate slab deck and CFS edge trim are needed to be assembled part-by-part. Beam and column members were fabricated with two

cold-formed steel lipped-channel sections back-to-back and fastened by using 12 mm of grade 8.8 bolts to create an I-shaped, respectively. Four of the test specimens—specimens 1 to 4—used a 0.90 m long beam section and only one specimen—specimen 5—used a 0.75 m long beam section. However, all specimens consisted of the column member by 1.50 m height with a constant thickness of 2 mm. The selection of size and geometry of the CFS beam and column members are due to the ‘scale down’ factor, which is able to represent the approximate length of the hogging moment (700 mm distance of the applied axial load) that occurred on the sub-assembly steel frame as suggested by Amsyar et al. (2021). According to Foraboschi (2019), a column either reinforced concrete or steel frame, by its definition, is a vertical support member loaded in compression. Any other loading conditions and effects shall be taken into account in design, such as lateral loading, global buckling and imperfections, which entail the interaction of flexure and compression in a geometrically non-linear regime (Foraboschi, 2019). In addition, Kang and Tan (2015) have suggested that in order to fit the extracted sub-assembly within the physical constraints of the laboratory in Nanyang Technological University, steel beam and columns section in the prototype building were scaled down to one-half, but the beam reinforcement ratio remained unchanged. Therefore, for the scaled down factor, Kang and Tan (2015) have proposed that the spacing of precast columns in two orthogonal directions was 3 m, and the dimensions of beams and columns were scaled down to 150 mm × 300 mm and 250 mm × 250 mm, respectively. Figure 1 illustrates the sample of detailing of precast concrete beam-column sub-assemblages after

considering the ‘scaling down’ factor prepared by Kang and Tan (2015).

Arrangement of reinforcing bars installed for all of the test specimens is specified in this study. As general, test specimen 1 to specimen 4 are using both transverse and longitudinal reinforcing bars (long product of steel) to be embedded into concrete slab. Specimen 1 used 10 mm diameter of high-strength steel reinforcing bar (T-bar). Meanwhile, specimen 2 used 8 mm diameter of mild-strength steel reinforcing bar (R-bar) embedded into the concrete slab. Specimen 3 and specimen 4 used the same mild-strength steel reinforcing bar (R-bar), but with a 10 mm diameter. However, specimen 5 used high-strength steel wire mesh (BRC) with 100 × 100 mm spacing and 900 mm length installed from the front flanges of the column section till the end span of the concrete slab. Therefore, apart from the other test specimens, only composite specimen 5 is using different arrangement of reinforcements in this study. Figure 2 demonstrates the type of arrangement of rebars for specimen 5 as compared to the other test specimens. The effect of arrangement of reinforcing bars on the structural behaviour of the composite CFS joint was investigated through the comparisons between specimen 1–4 and specimen 5. The height of reinforcement from the top of beam member was intended to be 75 mm and 100 mm for the 100 mm and 125 mm thickness of concrete slab, respectively. These specimens comprised three groups; these groups had rebar of different diameters, varying types of reinforcing bar and different slab thickness, as shown in Table 1. As for the composite CFS joint, HRS gusset plate with a dimension of 400 mm × 150 mm × 2 mm was slipped in at the beam and

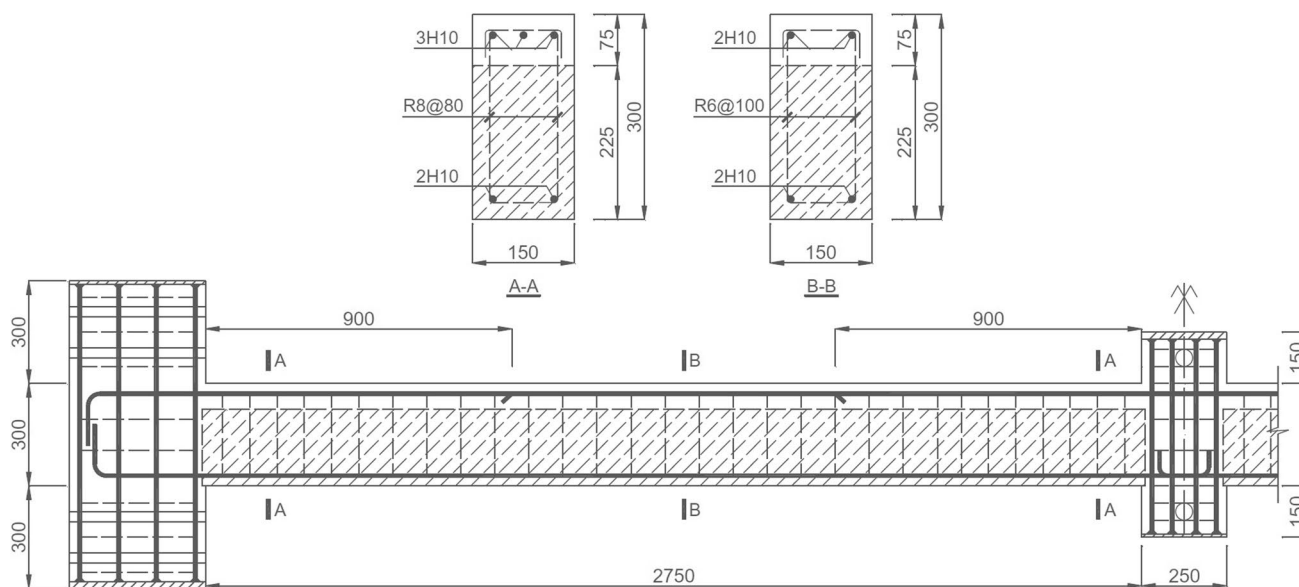


Fig. 1 Detailing sample of precast concrete beam-column sub-assemblages after considering the ‘scale down’ factor (proposed by Kang & Tan, 2015)

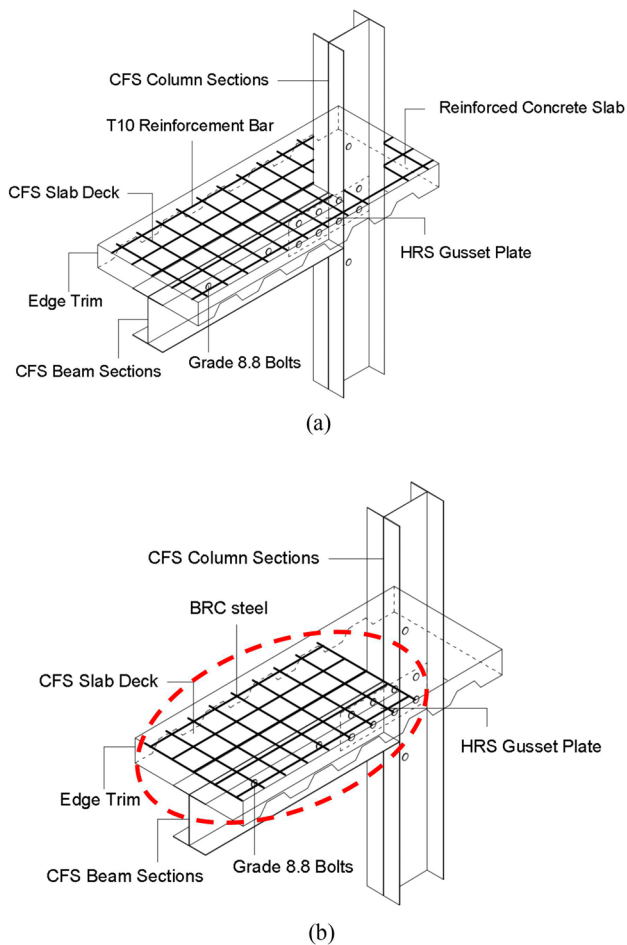


Fig. 2 3-D AutoCAD drawings of composite test specimens based on the arrangement of reinforcing bars: **a** Specimens 1, 2, 3 and 4 using long product steel rebars, **b** Specimen 5 using steel wire mesh (BRC) as reinforcement

column interface, which was fastened by using 12 mm diameter of grade 8.8 bolts by an arrangement of 50 mm from

both ends and 100 mm spacing. A slip-in connection from a notched beam was explored by Tahir and Siang (2008), who discovered that the 2 mm HRS gusset plate failed in lateral buckling before achieving the desired moment resistance. In this study, the author proposed a simpler, rectangular HRS gusset plate (J4-HG) with 2 mm thickness for the composite connection design. Meanwhile, installation of the CFS profiled slab deck and the 1 mm thick edge trim to act as a formwork for concreting slab was placed through the top of CFS column sections and lay down onto the upper flanges of beam members. Two modified ‘T-shaped’ of CFS shear connectors were slip-in and bolted along the back-to-back assembled CFS beam channel section with a distance of 300 mm from the beam edge. The fabrication of modified shear connectors is important for the composite action acting between the concrete slab and the steel structural members. The upper part of the installed shear connectors will be embedded into the concrete slab during casting or concreting work and the bottom part will be bolted and tighten up at the middle web section of CFS beam member. Figure 3 illustrates the diagram of connection between the profiled slab deck and the CFS beam in (a) 2D AutoCAD drawing details of shear connector, (b) 2D AutoCAD drawing details of CFS profiled slab deck and (c) Experimental preparation. Meanwhile, Fig. 4 displays the 2-D animation of the isolated CFS beam-to-column connection for both Auto-CAD drawing and ABAQUS modelling. The definition of its terms are: D_{beam} is denoted as the depth of the connected steel beam section, D_{col} denoted as the depth of steel column section, L_g is denoted as the length of the HRS gusset plate, B_g is denoted as width of the HRS gusset plate, t_g is denoted as thickness of the HRS gusset plate, e_1, e_2 are denoted as the edge distance from the centre of bolt hole and e_{p1}, e_{p2}, e_{p3} are denoted as the distance between centre-to-centre of the bolt holes.

All tensile tests were carried out in the D04, Structures and Materials Laboratory, School of Civil Engineering,

Table 1 Experimental specimen details

Spec	Column size (mm) ^a	Beam size (mm) ^a	Reinforcement (type, diameter)	Slab thickness (mm) ^b	Gusset plate size ^c	No. of bolts
1	200 × 150 × 1500	200 × 150 × 900	T10-bar	100-C30	400 × 150 × 2 – S275	8
2	200 × 150 × 1500	200 × 150 × 900	R8-bar	100-C30	400 × 150 × 2 – S275	8
3	200 × 150 × 1500	200 × 150 × 900	R10-bar	100-C30	400 × 150 × 2 – S275	8
4	200 × 150 × 1500	200 × 150 × 900	R10-bar	125-C30	400 × 150 × 2 – S275	8
5	200 × 150 × 1500	200 × 150 × 750	T10-BRC-wire mesh	100-C25	400 × 150 × 2 – S275	8

^aThe dimension of beam and column members are denoted as (depth × width × length) according to the manufacturer’s specification. All sections are 2 mm thickness with design yield strength of 468.2 N/mm²

^bSpecimens 1, 2, 3, 4 are using grade C30 of concrete meanwhile specimen 5 is using grade C25 for slab. All specimens are using 50 mm of concrete cover, C_{nom}

^cGusset plate size is labelled as (length × width × thickness – steel grade)

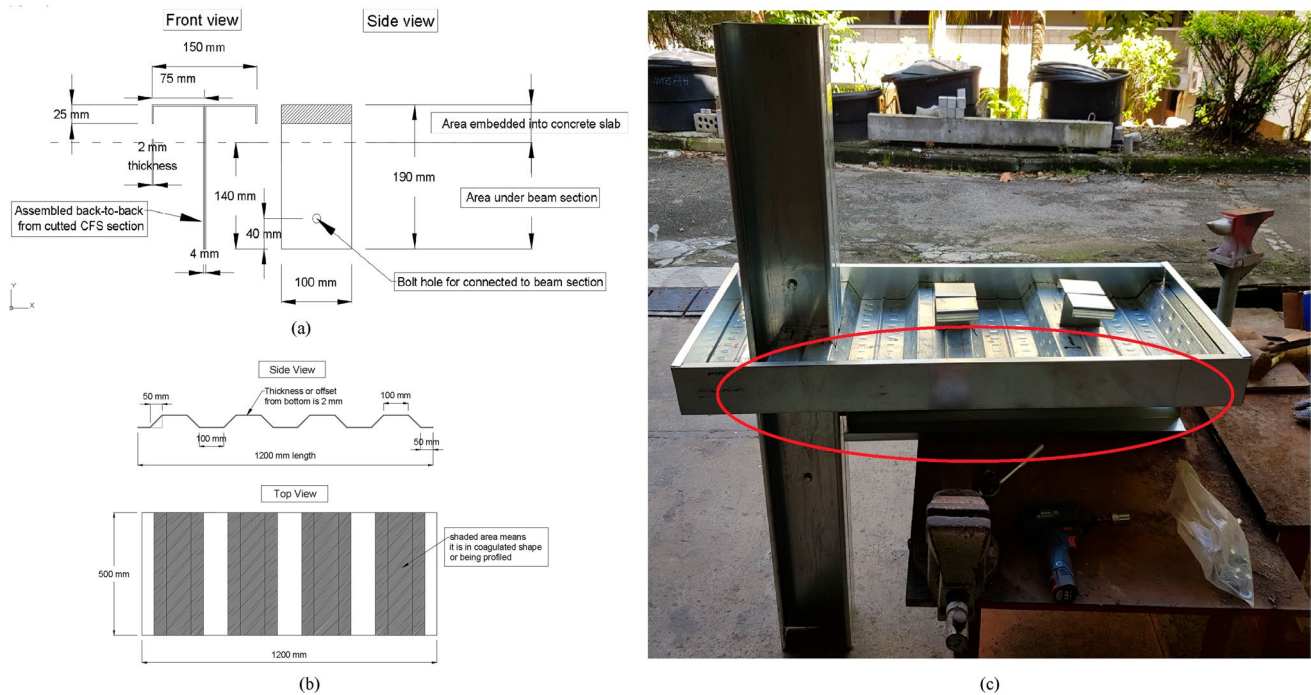


Fig. 3 Diagram of connection between the profiled slab deck and the CFS beam in **a** 2D AutoCAD drawing details of shear connector, **b** 2D AutoCAD drawing details of CFS profiled slab deck and **c** experimental preparation

Faculty of Engineering, Universiti Teknologi Malaysia. Mechanical properties of all reinforcing bars and CFS coupon plates were validated through the tensile strength test. The tensile test was conducted by using the SOP Tinius Olsen universal testing machine (UTM) in accordance with the BS EN ISO 6892-1:2016 (Part 1: Method of test at room temperature – metallic materials). Figure 5a and b illustrate the stress–strain diagrams for the cold-formed steel coupon plate and all reinforcing bars (R-bar and T-bar), respectively. Meanwhile, Table 2 details the mechanical properties of all steels involved in this study and test results were compared with design strengths to obtain strength ratios. Three sets of samples were prepared for each steel group so that the average of Young’s modulus of elasticity, yield and ultimate strengths can be calculated. Test results showed that actual strength of reinforcing bars and CFS coupon plate were beyond the design strength obtained from the manufacturer’s specification as the tensile strength ratios were ranged from 1.12 to 1.54. Furthermore, tension strength of 911.0 N/mm² of the bolt/fastener installed with two washers was used in this study to fasten the joint of steel frames. As for the concrete material, compressive strength test (cube test) was carried out in accordance with the BS EN 12390:2009—Part 1–8 to determine the compressive strength of the concrete cubes based on 7-day and 28-day ages. Two sizes of concrete cubes were used to conduct the compressive strength test, which were (100 × 100 × 100) mm³ and (150 × 150 × 150) mm³. Cube strength test was carried out on the same day of

isolated joint test was conducted. Table 3 summarizes the compressive strength results of the normal-weight concrete based on 7-day and 28-day ages. It was concluded that all of the tested concrete cubes exceeded the standard of 30 MPa strength for structural purpose in accordance to the BS EN 12390:2009.

2.2 Experiment Procedures

A total of five specimens were carried out in this study in order to investigate the joint behaviour and capacity of the proposed composite CFS beam-to-column joints. Isolated joint test was carried out by inducing single point load (axial load) to the composite CFS specimens. Bending in beam member was produced by the load applied at the cantilever with a distance of 700 mm for specimen 1–specimen 4, and 600 mm for specimen 5, acting from the load application to beam-column interface. A 100 kN capacity hydraulic jack was installed on top of the concrete slab to apply axial load and recorded by a load cell. Two digital inclinometers were fabricated near to the connection at the centre of column and beam web depth, respectively, so as to record the rotation of both steel members. Four linear variable displacement transducers (LVDTs) were positioned near to the centre of gravity for both beam and column sections. The testing configuration is shown in Fig. 6a. Actual layout of the testing specimen is illustrated in Fig. 6b. At the beginning, load application was applied with the increments controlled

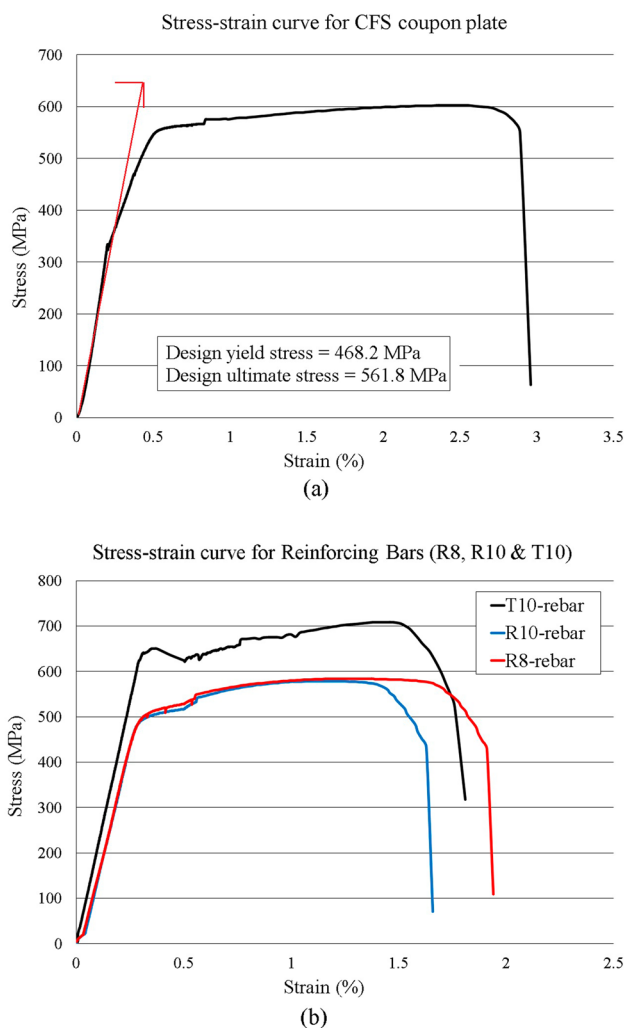


Fig. 5 Tensile stress–strain curves of the tested steel components: **a** CFS coupon plate, **b** reinforcing bars (R-bar and T-bar)

by load interval of 0.50 kN. As the readings of deflection were observed to be more significant, the load application was then controlled by the increments of deflection with an interval of 3 mm. The stabilized applied load and deflection of test specimens after 30–45 s intervals were recorded

and channelled to the tabular data stream (TDS-530) software through a high-speed data logger and connected to a computer.

3 Finite Element Model

3.1 Design of Composite Steel Components

All steel and concrete components involved in the composite CFS joint are using the 3-D modelling space with deformable type and solid extrusion for base feature. 1000 initial approximate size of 3-D space design is used in ABAQUS software to create both steel and concrete components. All of the main elements such as C-section beam and column members, HRS gusset plate, square 10 mm thick loading plate, modified CFS shear connectors, CFS profiled slab deck, grade 8.8 bolts and longitudinal and transverse reinforcing bars were designed as of the experimental program, with exact dimension and geometry in order to achieve precise computational analysis versus laboratory data. Meanwhile for the concrete part, normal-weight concrete was designed using space area to represent real condition of composite steel–concrete joints. All of the designated components were illustrated in Fig. 7. A 3-D deformable shell extrusion is used to create element in order to allow the cracking onto the concrete slab during the numerical analysis. A 1 mm depth of crack shell element is designated to all composite specimens so that identical parameter and crack distribution can be initially triggered to the concrete slab during simulation process. Partitioning all of the involved components in composite CFS model need to be perfectly done in order to perform smooth meshing and mass distribution. Appointing relevant datum points to the respective components is essential for the assembling process. It can be created by entering the respective coordinates for datum point in the ABAQUS’s command section – for instance by creating two points inside the concrete slab as a reference to relocate or translating the embedded reinforcing bars in both longitudinal and transverse directions. A datum point with 700 mm

Table 2 Mechanical properties of the cold-formed steel (CFS) coupon plate and reinforcing bars

Sample	Thick-ness (mm)	Diameter (mm)	Modulus of Elasticity (N/mm ²)	Design Strength		Tensile Strength Test		Strength ratio, <i>e</i> (Exp./Theo.) ^a
				Yield (N/mm ²)	Ultimate (N/mm ²)	Yield (N/mm ²)	Ultimate (N/mm ²)	
CFS coupon plate	2.0	–	1.81 × 10 ⁵	468.2	561.8	577.0	625.0	1.23
R8-rebar (G250)	–	8.0	1.85 × 10 ⁵	344.0	461.0	530.0	584.0	1.54
R10-rebar (G250)	–	10.0	1.97 × 10 ⁵	362.5	487.3	517.0	579.0	1.43
T10-rebar (G500)	–	10.0	2.15 × 10 ⁵	557.8	629.2	624.0	709.0	1.12

^aThe strength ratio is calculated based on the yield strength of the coupon plate or reinforcing bars obtained from the experimental tensile strength test divided by the design strength achieved from the manufacturer’s specification

Table 3 Compressive strength of the normal-weight concrete based on 7-day and 28-day ages

No. of days	No. of concrete cube tested	Average of compressive strength (MPa) ^a		Percentage of differences (%)
		100×100×100 (mm ³)	150×150×150 (mm ³)	
7 Days	4	32.86	32.23	1.92
16 Days (specimen 1)	3	38.15	36.74	3.70
20 Days (specimen 2)	3	40.02	30.21	24.51
20 Days (specimen 3)	4	41.25	32.34	21.84
22 Days (specimen 4)	3	38.36	42.14	9.85
28 Days	4	41.79	43.61	4.36

^aThe average compressive strength for both sizes of concrete cubes were exceeded the standard of 30 MPa strength for the purpose of structural in accordance to the BS EN 12390:2009—Part 1–8

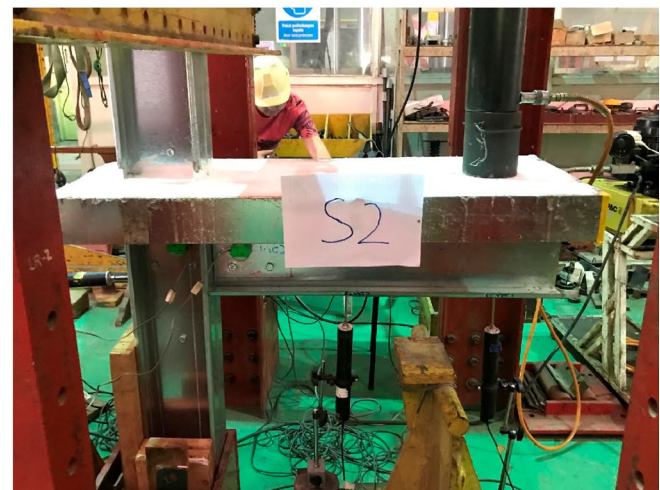
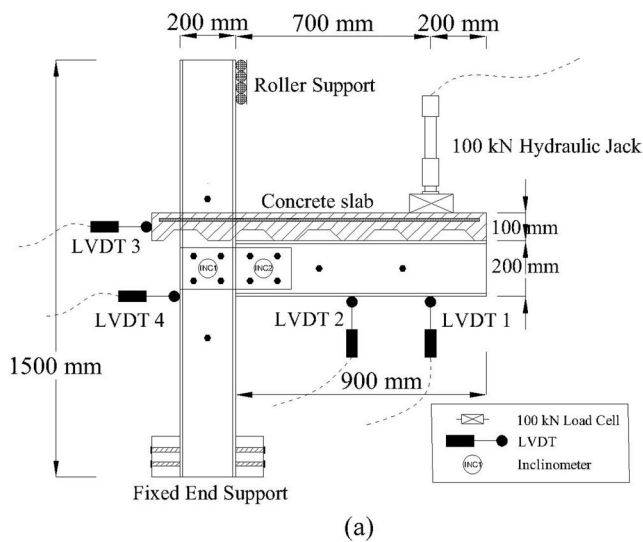


Fig. 6 General set-up and instrumentation of the composite CFS connection: **a** 2D sketch-up for isolated joint test, **b** Actual layout from the side view of the specimen

distance in x-direction from the front flange of the column section was created in this numerical works to submit the axial point load.

3.2 Material Models for Steel and Concrete Elements

According to Gao and Moen (2010), residual stresses formed by the CFS section is resulted by cold bending effect due to the imbalance between the partially plastic stress distribution and the elastic stress distribution from the unloading. It has been observed that the existence of the cold bending residual stresses is measured at the bent corners of square cold-formed HSS sections and Cee-sections and in the roller-bent wide flange structural steel beams (Weng & Pekoz, 1990; Batista & Rodrigues, 1992; Spoorenberg et al., 2010). However, some of the previous researchers have ignored to the effect of the cold bending and some of them have

recommended to include the modelling protocols with the residual stress and an increased yield stress at the cold-bent locations of a member cross-section. The mechanics that define cold bending residual stresses and plastic strains are introduced, including the classical metal plasticity laws, e.g. isotropic and kinematic hardening, which play an important role in simulating the structural behaviour including the influence of the cold bending. In this study, for the numerical investigations and material properties input, isotropic elastic with ‘long-term’ moduli time scale (for viscoelasticity) is set for the elastic properties. Meanwhile, isotropic hardening plastic option is selected to the plastic properties by specifying both yield and ultimate strengths with plastic strain values. All steel and concrete components need to be assigned to its material properties, for instance properties of mass density, elastic–plastic behaviours and crack specification for concrete material. Von Mises’ plasticity was used to model all structural steel parts due to it performed as an

elastic–plastic material with strain hardening in both tension and compression. ‘Homogeneous’ solid section to the 3-D solid element is created to all components except for the crack element which is in 2-D formable shell. Table 4 tabulates the material properties for each of the involved components in composite CFS model for numerical modelling. According to Prabha et al. (2018), steel was assumed to behave as an elasto–plastic material in tension and was typically represented by a multi-linear constitutive model in the computational simulation. “Elastic” and “Plastic” normal behaviours were selected from the ABAQUS material library to define the elastic and plastic characteristics of the stress–strain curve. The results from tensile coupon tests by using SOP Tinius Olsen Universal Testing Machine (UTM) are selected for the data input of steel properties in ABAQUS software. The values of nominal stress (σ_n) and nominal strain (ϵ_n) obtained from the conventional tensile test were initially converted into the true stress (σ_t) and true strain (ϵ_t) by using Eqs. (1) and (2), respectively, due to the nominal stress–strain (σ_n – ϵ_n) curve obtained in the test did not give a true indication of the deformation characteristics of a material at higher strain.

Damage for traction separation laws with “Maxps Damage” was proposed to be the best and appropriate option for the concrete preferences rather than the concrete damaged plasticity setting. The proposed approach was carried out in this study as it allowed cracking development to interfere the model analysis by making sure that the concrete component underwent actual condition as those with physical laboratory tests. For normal mode fracture energy, “energy” option with “linear” softening type was specified for the damage evolution. Meanwhile, for the elastic part of the stress–strain curve, the values of Young’s modulus of elasticity (E) and Poisson’s ratio (ν) for the concrete were 3.5×10^4 N/mm² and 0.20, respectively. “Mass density” configuration from the ABAQUS library was assigned to both steel and concrete components to specify its density characteristic. Design of the 2-D crack ignition for crack growth throughout the concrete slab was initially assembled to the present model for the “XFEM” method.

$$\sigma_{true} = \sigma_{engineering}(1 + \epsilon_{engineering}) \quad (1)$$

$$\epsilon_{true} = \ln(1 + \epsilon_{engineering}) \quad (2)$$

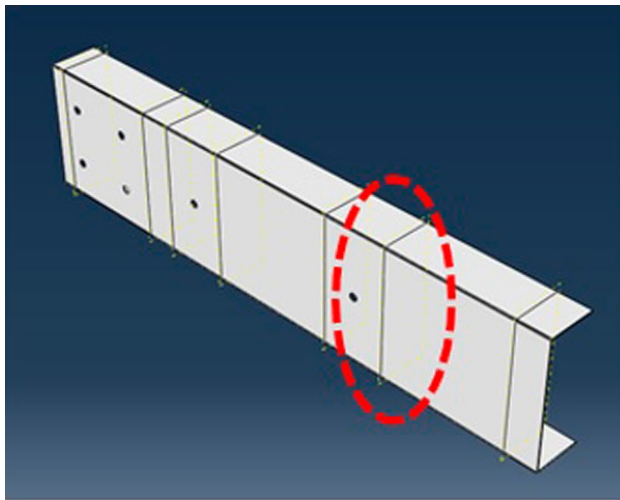
3.3 Assembling of Model Components

The process of assembling all of the created parts or components in ABAQUS is a process of where fabricating or re-assembling the steel and concrete components taking place in the assembling area, using the assigned datum point (x, y, z) coordinates by translating or rotating options, depending

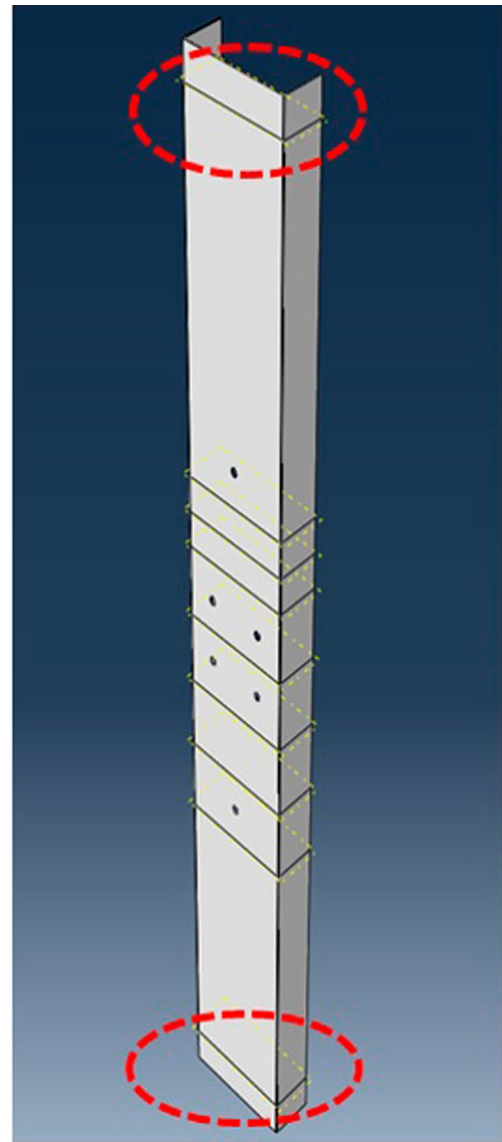
on the position and geometry of the element to be assembled. First step of assembling is to create the instance from the parts or models, and assign the dependent instance type to all components. ‘Coaxial’ and ‘face-to-face constraint’ options in the ABAQUS library were used in the assembling process. First, the ‘coaxial’ option needs to be considered to all tension bolts onto the inner surfaces of the bolt holes assigned to the beam, column and slip-in HRS gusset plate elements. ‘Face-to-face constraint’ option is then used to assign to the inner surfaces of the bolt head to the outer surfaces of the connected components, for instance, tension bolts to the beam section, in order to assemble the material into one structure beam; from back-to-back assemble. Reference point is also required in the modelling assembly as it can be assigned to any interest of point, for example, reference point needs to be created at the symmetry upper surface of the loading plate element, for appointing the concentration load and not using the pressure option provided. For the proposed composite model, a total of 41 instances must be assembled together to form a complete isolated composite CFS joint model, with the integration of 60 position constraints mainly for the ‘coaxial’ and ‘face-to-face’ constraints.

3.4 Contact Interactions

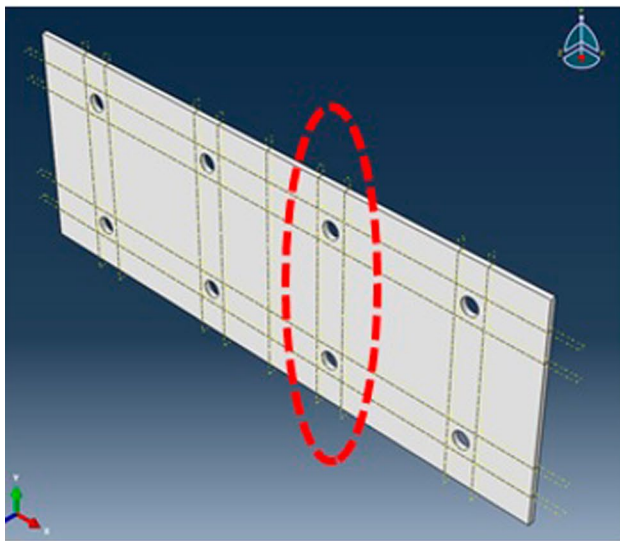
A new approach and technique for the model contact interaction, element constraint and cracking mechanism were proposed in this study to simulate the proposed model. Small sliding formulation with “surface-to-surface” contact was assigned to the critical surface interactions, such as the interface between beam–column flanges, slip in HRS gusset plate with column–beam web surfaces and bottom surface of the concrete slab with top flange of beam sections. Two interaction properties available in the ABAQUS library were seemed to be the most suitable options to simulate the model. Tangential behaviour with 0.3–0.6 friction coefficient was adopted and normal behaviour with “Hard” contact pressure-over closure was selected to consider the interaction properties. The penalty friction formulation for tangential behaviour is applied with two different friction coefficients of 0.3 and 0.5, where 0.3 is applied between the web surfaces of beam and column with slip-in of HRS gusset plate and shear connectors, while 0.5 coefficient value is applied between the flange surfaces of steel beam with CFS profiled slab deck. Analytically, the larger surface between two parts in interaction will act as the master surface and the other as the slave surface. Throughout the modelling, column as main component will act as a master surface, followed by the beam section, profiled slab deck and other parts. Adopting the normal “Hard” contact pressure-over closure was essential in this simulation to eliminate any penetration occurrence of the slave–master surfaces during



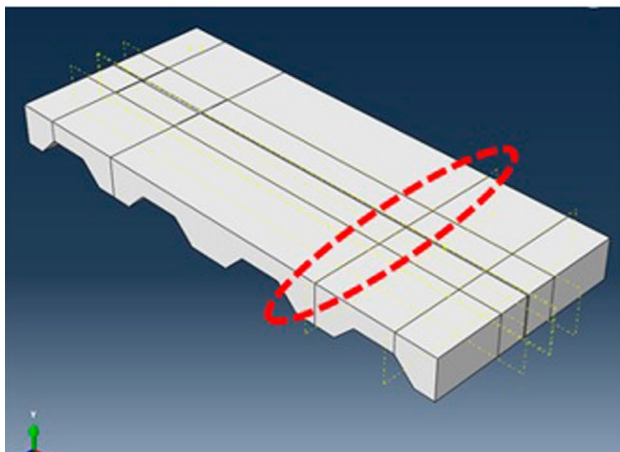
(a)



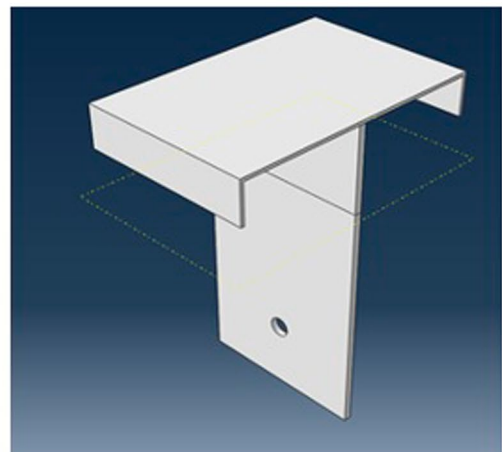
(b)



(c)



(d)



(e)

Fig. 7 All steel and concrete components that involved to form a composite CFS model: **a** CFS beam section with 7 partitions, **b** CFS column section with 9 partitions, **c** HRS gusset plate with 13 partitions, **d** 100×500×1200 mm concrete slab, **e** 150×190 mm modified CFS shear connectors

full analysis. Full composite action between CFS beam and concrete slab was assumed by using shear connectors, which were omitted in the FE analysis. The same approach of surface-to-surface contact interaction with “Hard” properties was applied to the interaction of shear connector and beam web bottom areas. Meanwhile, “embedded region” option was selected in this study to merge the upper element of shear connectors to the concrete slab and embedding R-bar, T-bar and BRC reinforcing bars into a concrete structure. “XFEM” crack growth for concrete cracks development was proposed in this model to forecast the actual failure mechanism with those in the laboratory test, which involved both longitudinal and transverse cracking. Figure 8 illustrates the typical FE model of the semi-rigid composite CFS joint with essential information of the contact interactions, load and boundary conditions.

3.5 Load and Boundary Conditions

FE analysis for the semi-rigid composite CFS joint model in ABAQUS software adopted the identical method of loading and boundary conditions to those configured in the laboratory tests. A 10 mm thick of loading plate with square dimension of 50 mm×50 mm was modelled and positioned on top of concrete surface with 700 mm distance apart from the beam-column connection to provide a reference point for equal load distribution during simulation process. “Pinned” and “Encastre” options were selected for the boundary conditions of the model as it provided a pin support to the upper region and fixed-end support to the bottom section of the column component with restricted z-axis direction. To perform the exact conditions with those in the experimental programme, column flanges and sides of the concrete were restricted to z-axis direction to provide bracings purpose so that the deflection or deformation will only be performed in x-axis and y-axis directions. To conduct the analysis by using displacement control instead of load control, 150 mm downward direction of displacement was assigned to ‘reference point 1’ to perform complete simulation with results to the unloading parts after reaching to the ultimate moment resistance of the curves drawn by the FE analyses.

3.6 Element Type and Mesh Discretisation

Convergence problem under bending conditions is one of the common issues that occur during selection of element types and size of global meshing, especially to the concrete

component. To overcome this problem, mesh convergence needs to be carried out to each of the involved components by specifying a set range of mesh size so that a suitable and optimal meshing can be obtained with reasonable computational time. A 3-D stress option with an eight-node linear brick element and no hourglass controls (C3D8) was proposed to simulate all steel and concrete components as it provided further analysis beyond ultimate load-bearing capacity with accurate results. Large deformation, contact, plasticity and failure conditions can be accounted for the non-linear analysis by using the 8-node brick elements with no reduced integration (C3D8). To get the magnitude of stress concentration accurately, finer mesh was assigned to complex areas, for instance, at the joint region and surface interaction between modules. A combination by using fine and coarse meshing sizes could be performed by determining suitable partition numbers to be assigned for each component to avoid convergence problem with affordable computational time.

4 Experimental Results and Discussion

4.1 Failure Mechanisms

In general, it was observed that almost identical cracking patterns were exhibited by all composite specimens. All tested samples had developed initial cracks on the concrete slab at the column front flange and below the loading position. Then initial cracks were continued with the development of transverse cracks at mid-span of concrete slab and expanded with longitudinal cracks at two-third of the ultimate load-bearing capacity. Concrete crushing was frequently detected at the ultimate resistance of the composite joint, as shown in Fig. 9. For specimen 5, it was observed that severe cracking failure is occurred during the isolated joint test compared to the other test specimens. The first observed failure pattern was concrete cracking across the direction of column on top of the concrete surface. As the applied point load increased, the crack was obviously propagated through the whole width of the concrete slab. On the other hand, it can be considered that specimen 5 was nearly acting as a non-composite CFS joint. All failure modes of the experimental programme shown in the Fig. 9 were compared side-by-side with the 2-D AutoCAD drawings, in order to provide a clearer sight for the crack development. Due to inadequate data fracture parameters in concrete modelling, the slight drop in applied load because of the crack development at mid-span and load position could not be clearly captured in FE analysis. Therefore, in the context of concrete, crack growth and propagation were not studied in-detail, as the main focus of this study was to evaluate the strength of the CFS joint structures. However, consideration

Table 4 Details of the material properties for the involved composite components in composite CFS model

Component(s)	Density (kg/mm ³)	Elastic properties (MPa)	Plastic properties (N/mm ² or MPa)
Cold-formed steel (CFS) section	7.065×10^{-9}	Y.M.: 2.1×10^5 Poisson's ratio: 0.3	Y.S.: 468.20, P.S.: 0.00 U.S.: 561.80, P.S.: 0.03
Hot-rolled steel (HRS) gusset plate	4.800×10^{-9}	Y.M.: 2.1×10^5 Poisson's ratio: 0.3	Y.S.: 275.00, P.S.: 0.00 U.S.: 410.00, P.S.: 0.03
10 mm square loading plate	4.800×10^{-9}	Y.M.: 2.1×10^5 Poisson's ratio: 0.3	Y.S.: 275.00, P.S.: 0.00 U.S.: 410.00, P.S.: 0.03
CFS shear connector	7.065×10^{-9}	Y.M.: 2.1×10^5 Poisson's ratio: 0.3	Y.S.: 468.20, P.S.: 0.00 U.S.: 561.80, P.S.: 0.03
T10 reinforcement bar	6.080×10^{-9}	Y.M.: 2.1×10^5 Poisson's ratio: 0.3	Y.S.: 554.80, P.S.: 0.00 U.S.: 629.20, P.S.: 0.03
Grade 8.8 tension bolt (12 mm diameter)	7.065×10^{-9}	Y.M.: 2.1×10^5 Poisson's ratio: 0.3	Y.S.: 850.00, P.S.: 0.00 U.S.: 911.00, P.S.: 0.03
Concrete slab with crack specification of 2400 kg/m ³ density	2.400×10^{-9}	Max principal Stress: 40.0 Y.M.: 3.5×10^4 Poisson's ratio: 0.2	N.M.F.E.: 4200 S.M.F.E.F.D.: 4200 S.M.F.E.S.D.: 4200 Viscosity coef.: 0.0001

1. Y.M. denoted as Young's Modulus of Elasticity of the material. 2. Y.S. denoted as yield strength of the material. 3. P.S. denoted as plastic strain respected to the stress (yield and ultimate stress). 4. U.S. denoted as ultimate strength of the material. 5. N.M.F.E. denoted as normal mode fracture energy. 6. S.M.F.E.F.D denoted as shear mode fracture energy first direction. 7. S.M.F.E.S.D denoted as shear mode fracture energy second direction. 8. Viscosity coef. denoted as viscosity coefficient

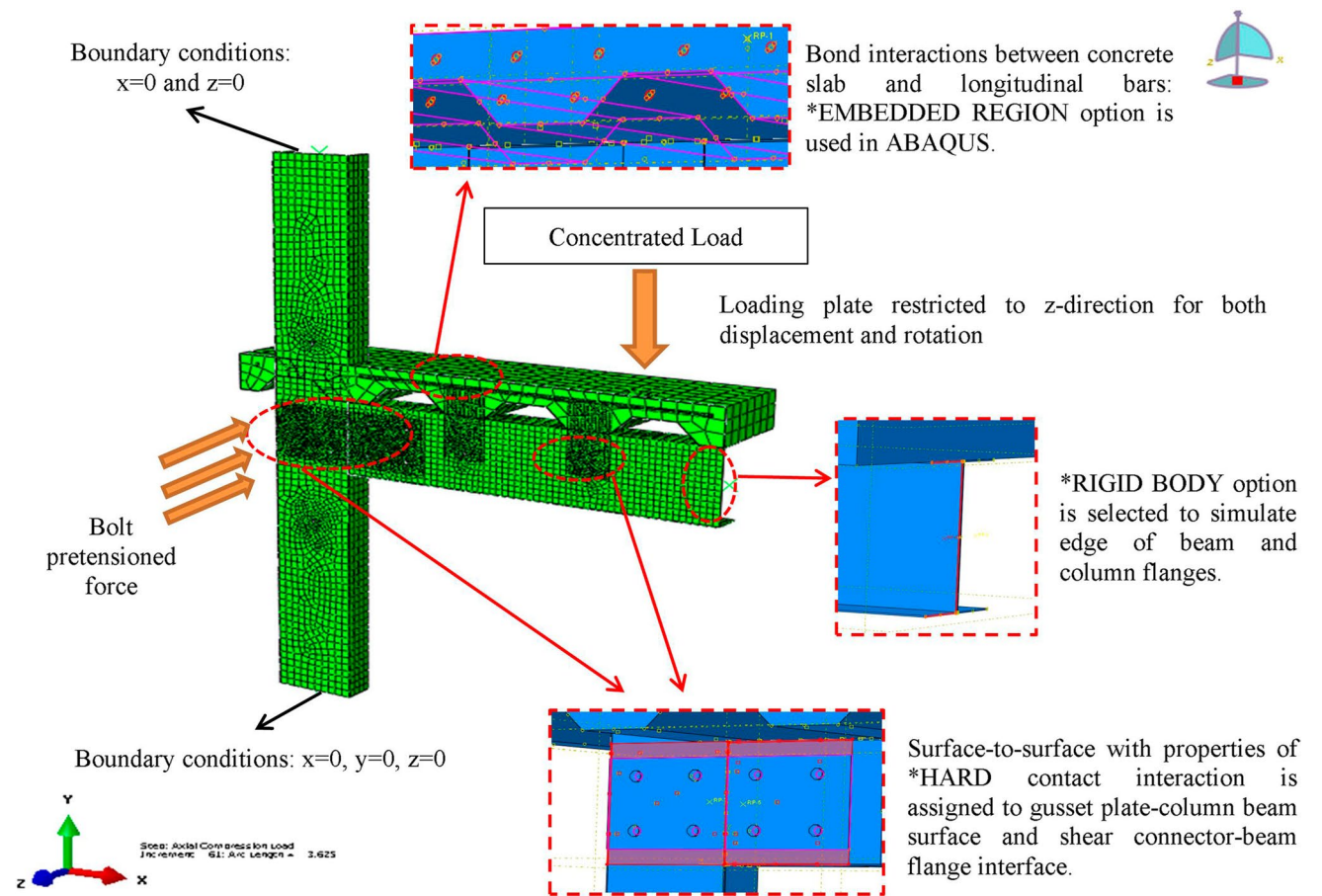


Fig. 8 FE model of a typical composite CFS connection with all conditions

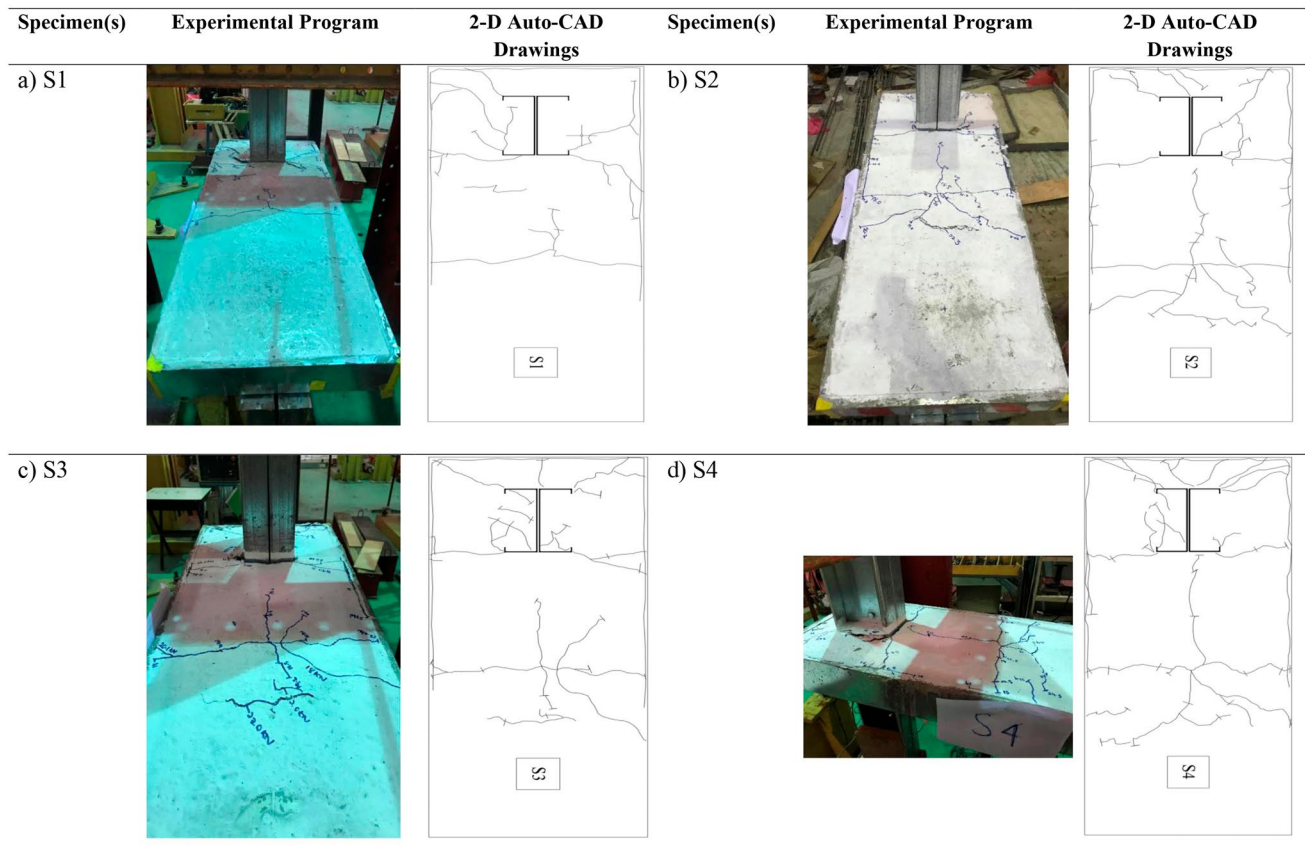


Fig. 9 Comparisons of side-by-side 2-D AutoCAD drawings and real-time isolated joint tests, showing the crack development for all composite CFS joint specimens: **a** Specimen 1, **b** Specimen 2, **c** Specimen 3 and **d** Specimen 4

of crack ignition to the model was conducted through the modelling, firstly to predict the initial location of the cracking from the experimental observations. It is observed that the initial cracking was occurred at the area of the beam-column interface, specifically at the front flanges of column section, whereas the tension zone was captured as indicated in the component method theoretically. Local buckling of CFS members is a typical failure that being observed through all of the laboratory tests, especially to the column sections. Several other deformations were identified during the physical tests and numerical analysis and were reported as below:

- i. Bearing failure in the section web around the bolt hole;
- ii. Local buckling of the CFS column flange, as shown in Fig. 10a and b;
- iii. Deformation of the HRS gusset plate, as illustrated in Fig. 11a.

In almost all specimens, local buckling had occurred at the compression zone of column section. The specimen

was good at tension zone due to the factors of reinforcing bars embedded in concrete slab and gusset plate functioning as the interface connector. Load popping sounds were clearly heard during the experimental test. This happened to all specimens; the concrete seems to explode and pieces of mortar cement were observed to spit out from the slab during explosion. Based on visual inspection, the tension area of the concrete slab, which was near to the column of all specimens, started to crack when the applied load was approximated to 4.0 kN. The metal decking was not deformed when the ultimate load capacity was reached. Also, for the fasteners or bolts, high concentrated stress can be captured after computer simulation via the Von Mises' stress. However, there is no severe deformation occurred to the fasteners, as illustrated in Fig. 11b, and it is assumed that the accumulated stress displayed by the ABAQUS software is not beyond the actual strength of the bolts and able to withstand any further applied load to the bolted moment CFS joint structure.

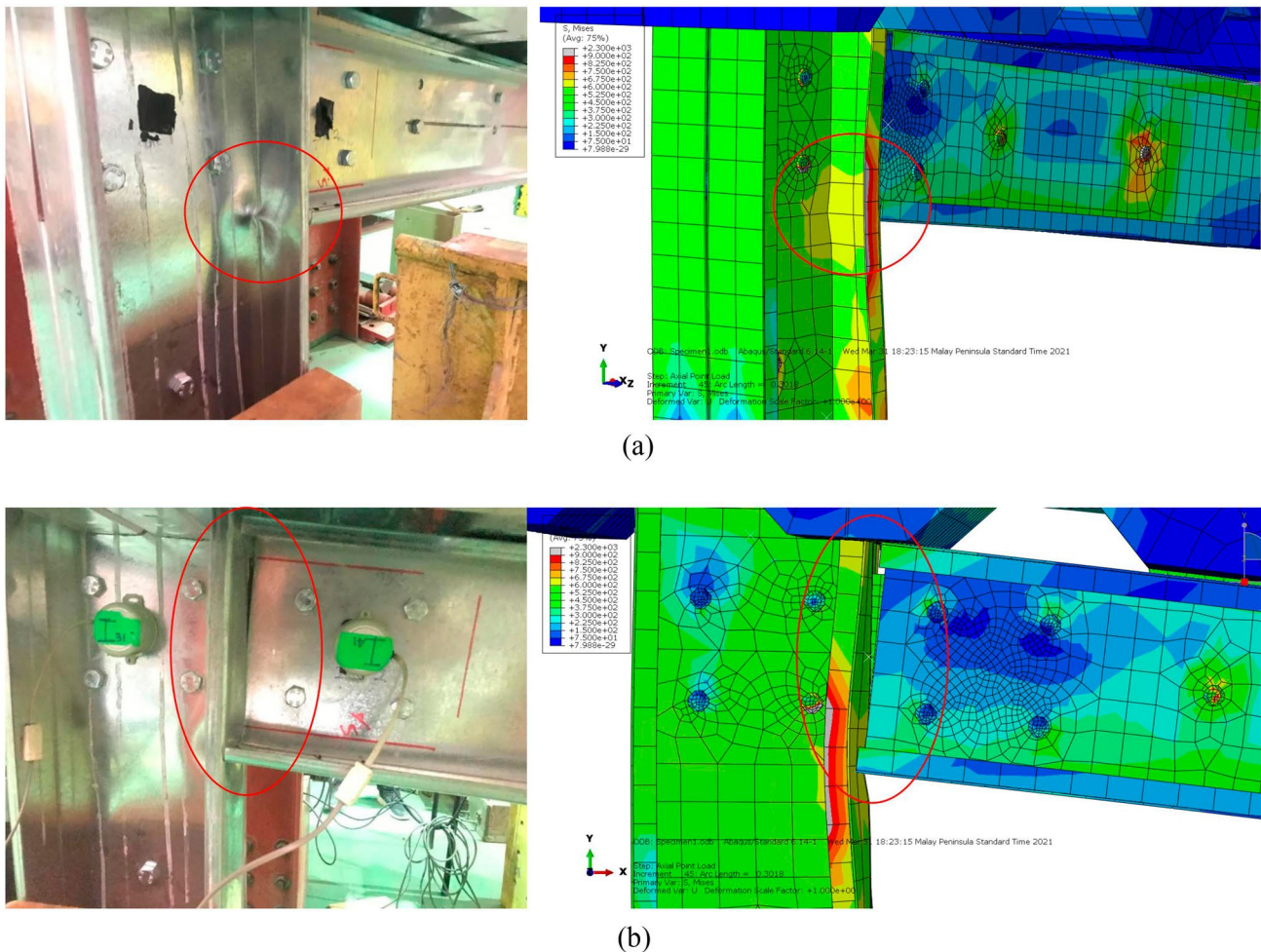


Fig. 10 Local buckling of the CFS column flanges illustrated by experimental and FE analyses

4.2 General Behaviour of Composite CFS Joint

4.2.1 Load–deflection Relationship

Load–deflection responses for all tested composite CFS joints are presented in Fig. 12a. Based on Fig. 12a, the overall respective trend for deflection was almost the same. This was due to the arrangement of the reinforcing bars for test specimens 1–4 were the same and obviously contributed to the composite action formed by integrating the CFS sections with concrete slab. For all specimens, deflection was increased proportionally to the increase in applied load. The ultimate loads attained for specimen 1, specimen 2, specimen 3 and specimen 4 were 23.80 kN, 22.60 kN, 23.30 kN and 25.10 kN, respectively. End deflections at ultimate loads level were recorded as 80.16 mm, 74.26 mm, 82.35 mm and 80.51 mm, respectively. As compared to specimen 5, which used the T10 of BRC steel wire mesh, the failure load was only at 14.0 kN, with corresponding deflection of 46.72 mm. The effect of arrangement of reinforcing bars

on the structural behaviour of the composite CFS joint was investigated through the comparisons between specimens 1–4 and specimen 5. As the specimens are unable to sustain any incremental load beyond its ultimate load-bearing capacity, significant drop of applied load and declination of curves can be seen in the graph.

4.2.2 Moment-rotation Responses

The behaviour of moment connections is typically represented by a moment-rotation curve, as shown in Fig. 12b. Through the experimental analysis, it was observed that a straight linear graph was exhibited by almost all composite CFS joint specimens in its elastic region, followed by a non-linear curvature in the plastic region and continuously losing its stiffness as the rotation was increased. A bilinear concept was considered in this study to determine the ultimate moment resistance and its initial rotational stiffness. The ultimate moment resistances attained from the experimental test of specimen 1, specimen 2, specimen 3 and specimen 4

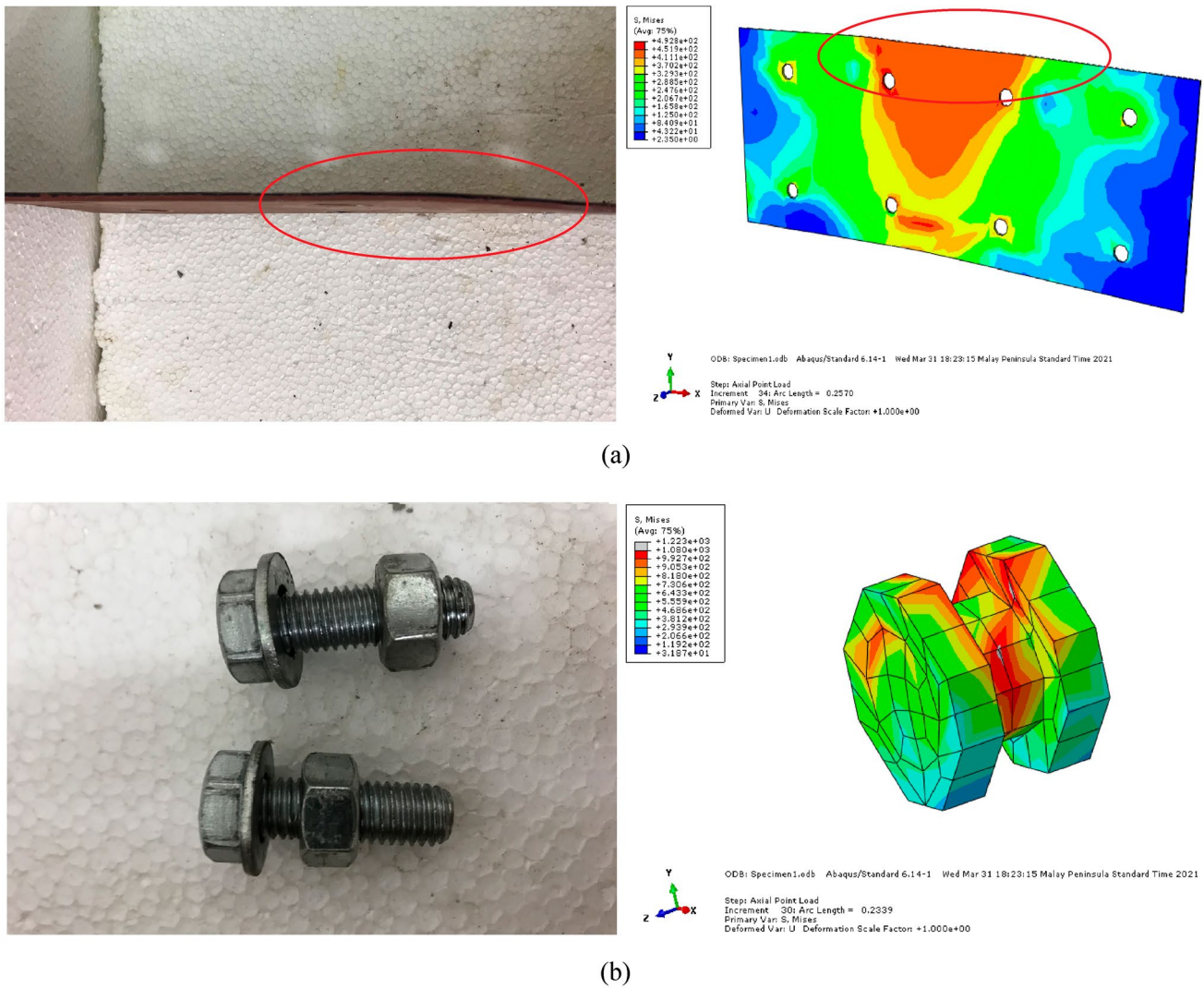


Fig. 11 Failure modes of steel materials: **a** Deformation of the HRS gusset plate illustrated from experimental and FE model, **b** Huge stress appeared at the bolt shank and inner surfaces of bolt head/nut

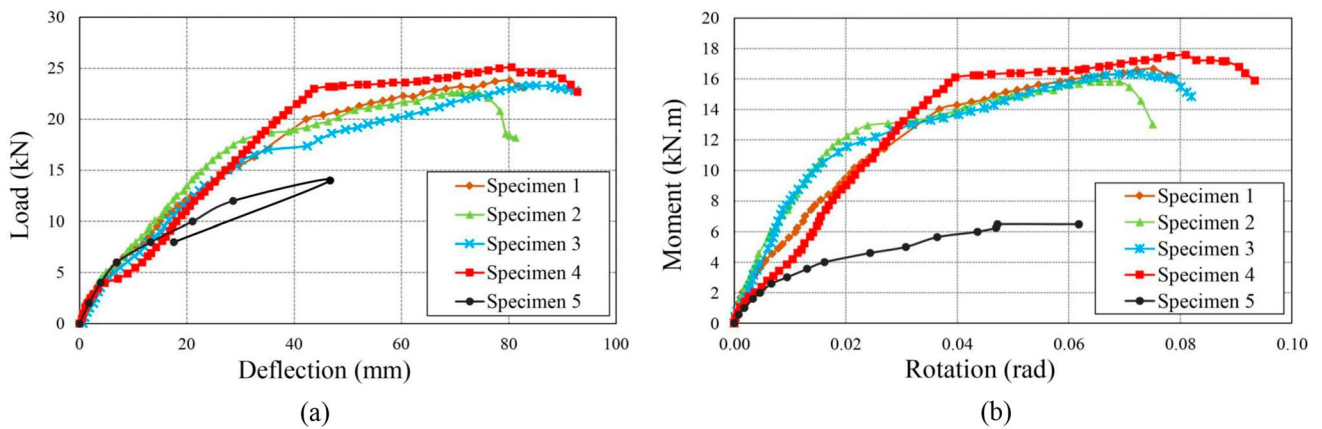


Fig. 12 **a** Load–deflection responses for all composite CFS joint specimens, **b** moment–rotation relationship for all composite CFS joint specimens

were 16.66 kNm, 15.82 kNm, 16.31 kNm and 17.57 kNm, respectively. Corresponding rotations at the ultimate moment resistances level were recorded as 0.075 rad, 0.067 rad, 0.073 rad and 0.081 rad, respectively. As compared to specimen 5, which used the T10 of BRC steel wire mesh, the ultimate moment capacity from experimental result was only 6.47 kNm, with a corresponding rotation of 0.062 rad. The initial rotational stiffness for specimen 1, specimen 2, specimen 3, specimen 4 and specimen 5 were calculated to be 520.5 kNm/rad, 712.6 kNm/rad, 756.8 kNm/rad, 424.2 kNm/rad and 500.0 kNm/rad, respectively. Since sufficient rotation was attained by all test specimens at more than 0.03 rad, the composite CFS joints had developed high ductility performance as sudden fracture was not observed in this study. The ratios of FEM to experimental ultimate strength varied from 0.92 to 0.98, as tabulated in Table 5. To simplify the findings and validations, it is required to satisfy $\frac{M_{j(fem)}}{M_{j(exp)}} \leq 1.0$. Engineers and structural designers, for examples, could be assured in evaluating the design strength while complying to safety requirements if there is a good and robust agreement between experimental and numerical analyses. Figure 13a–d displayed the comparisons of moment-rotation relationship between the experimental and FEM analysis results for specimen 1, specimen 2, specimen 3 and specimen 4, respectively. Agreement to the range of the strength ratios between FEM to experimental findings was acceptable to less than 1.0. This is due to some justifications such as taking the partial safety factor for reinforcement checking in tension zone, the standard design strength of the CFS sections (beam and column members) as compared to the tested mechanical tensile strength from the physical laboratory test. The design strength of the materials, for instance CFS beam and column sections was used based on the specification from the supplier. The design yield and ultimate strengths of the CFS section were defined by the values of 459 N/mm² and 549 N/mm², respectively. However, the yield and ultimate tensile strengths from the laboratory tensile test were obtained in the range of 523 N/mm²

and 625 N/mm², respectively. The increases of 13–25% of the mechanical strengths have resulted to the increases of the moment resistance for the composite CFS beam-to-column joint specimens in the experimental testing. In addition, calculation of the composite action between lightweight concrete slab with CFS beam members is not truly considered in the design component method.

4.3 Performance of the Semi-rigid Composite CFS Joint

4.3.1 Diameter of the Reinforcing Bars

To evaluate and discuss the laboratory results, different diameters of reinforcing bars used in specimen 1, specimen 2, specimen 3 and specimen 5 were tested. It was observed that the increase in diameter of reinforcing bar from 8 to 10 mm experienced an increase in the ultimate moment capacities from 15.82 to 16.66 kNm, with 5.31% higher capacity as compared to the composite CFS specimen with 8 mm diameter of rebar. The highest ultimate moment capacity was initially obtained by specimen with 10 mm of T-bar, followed by 10 mm and 8 mm of R-bar. However, specimen 5 which used T10 BRC steel wire mesh obtained the lowest ultimate moment resistance of 6.47 kNm. The results were significant due to the size of rebar and design strength of the steel had played an important factor to evaluate the capacity of connection at tension zone. According to Cao et al. (2021), sufficient bending capacity could be provided to the composite beam structure as two or more reinforcing bars were installed along the longitudinal direction to minimise the critical fracture of the encased concrete.

4.3.2 Types of the Reinforcing Bars

Testing of specimen 1, specimen 3 and specimen 5 were carried out to evaluate the performance of using different types of reinforcing bar in the composite CFS beam-to-column connections. It was found that the composite joints with

Table 5 Summary on the comparisons of experimental and FE analyses

Test reference	Details of specimen	Experimental results Ultimate Moment Capacity, $M_{j,exp}$ (kN m)	FEM results Ultimate moment $M_{j,fem}$ (kN m)	Strength ratio ^a
Specimen 1	T10-bar with slab—100 mm thickness	16.66	15.53	0.93
Specimen 2	R8-bar with slab—100 mm thickness	15.82	15.44	0.98
Specimen 3	R10-bar with slab—100 mm thickness	16.31	15.54	0.95
Specimen 4	R10-bar with slab—125 mm thickness	17.57	16.19	0.92
Specimen 5	T10 (BRC—wire mesh)—750 mm beam length	6.47	—	—

^aStrength ratio of moment resistance in this section is calculated by dividing FE analysis results to the experimental ultimate moment capacity of a connection

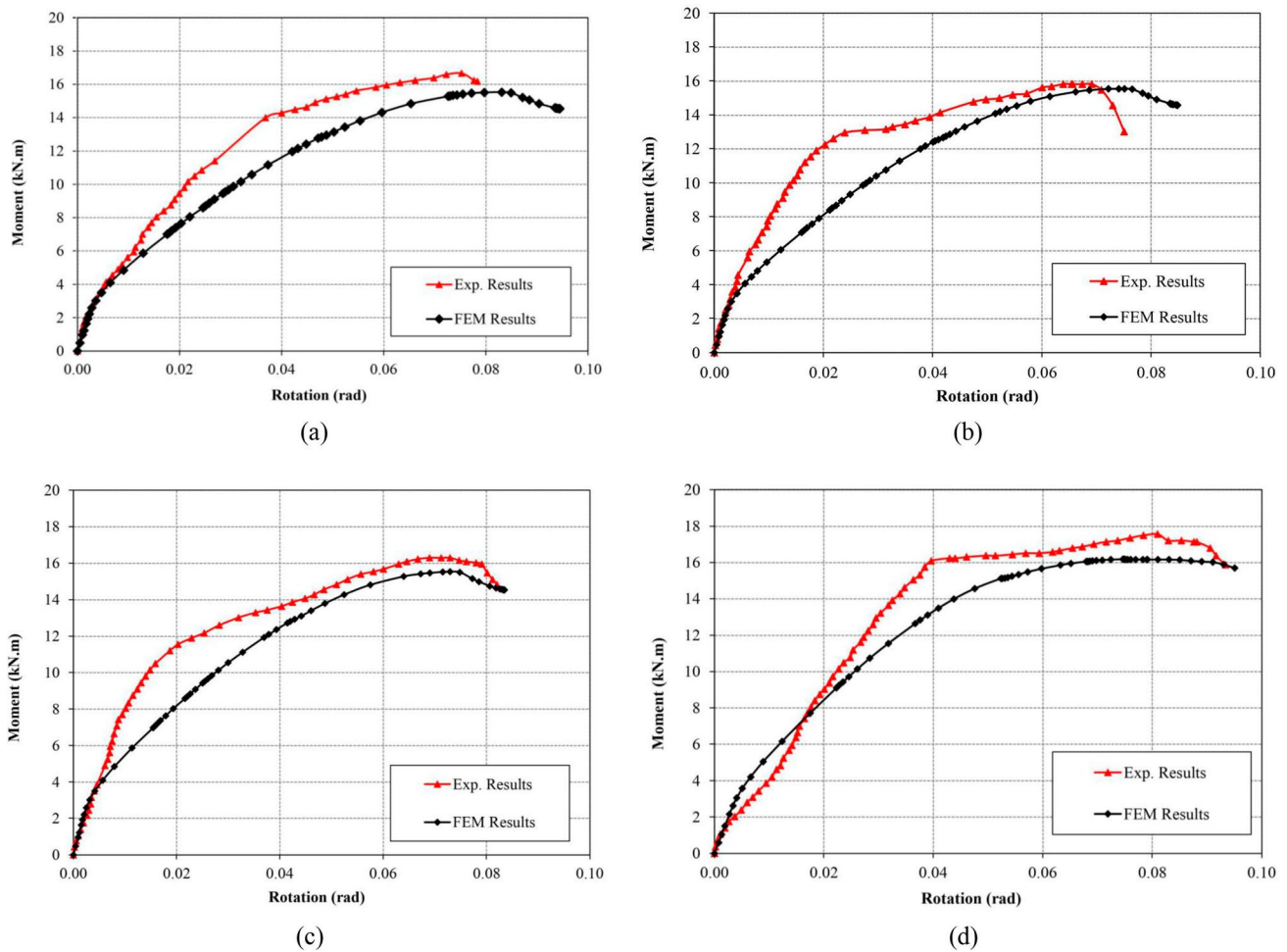


Fig. 13 Comparisons of the moment-rotation relationship between experimental and FEM results: **a** specimen 1, **b** specimen 2, **c** specimen 3, **d** specimen 4

high-strength steel reinforcing bar (T-bar) showed a slightly increase in ultimate moment capacity by 3%, as compared to specimen which used the mild-strength steel reinforcing bar (R-bar). Specimen 1 with T-bar had resulted in an ultimate capacity of 16.66 kNm, while Specimen 3 with R-bar had a maximum moment resistance of 16.31 kNm. However, specimen which used high-strength steel wire mesh (BRC) had resulted in the lowest ultimate moment capacity as compared to other tested specimens. This was because the design strength of the T-bar had performed higher yield strength as compared to the R-bar. Furthermore, the high-strength steel reinforcing bar (T-bar) was performed with physically irregular surface, while mild-strength steel reinforcing bar (R-bar) was made up of smooth rounded surface.

4.3.3 Thickness of the Concrete Slab

Specimen 3 and specimen 4 were tested in this study to evaluate the performance of using different slab thicknesses.

Based on the laboratory programme, specimen 3 was formed by using 100 mm thick of concrete slab and resulted with an ultimate moment resistance of 16.31 kNm. Meanwhile, specimen 4 attained a moment capacity of 17.57 kNm as its slab thickness was 125 mm. This result led to an increase of 8% of the ultimate moment capacity between specimen 3 and specimen 4. This was expected since capacity of the connection was increased proportionally to the increase in slab thickness due to enhancement of the compression zone in concrete structure.

5 Conclusion

An experimental and numerical study was performed to evaluate the structural behaviour of the semi-rigid composite CFS beam-to-column joints, in terms of its strength and stiffness. Mechanical properties of the CFS and all reinforcing bars were carried out through the tensile strength test

and the results showed that strength ratios were ranged from 1.12 to 1.54. The structural behaviour of the isolated joint specimens along the test progress was explained through the load versus deflection graph and moment against rotation relation. Through the experimental analysis, it can be observed that a straight linear graph was exhibited by almost all composite CFS joint specimens in its elastic region, followed by a non-linear curvature in the plastic region and continued to lose its stiffness as the rotation increased. Results showed that higher initial stiffness was associated with a higher moment resistance. Ultimate moment capacity was obtained by increasing the diameter of reinforcing bar, thickness of concrete slab and using high-strength steel reinforcing bar rather than the mild-strength steel rebar and high-strength steel wire mesh. Comparisons between laboratory and finite element analysis, which resulted in terms of ultimate moment resistance, showed a good correlation with strength ratios that ranged from 0.92 to 0.98. It is concluded that the proposed model created by using the ABAQUS software is proven to simulate the actual behaviour of partial strength composite beam-to-column CFS joint and is closely capable of predicting the ultimate resistance of test specimens. It was proven that using the simulation software, such as ABAQUS or ANSYS, it enabled evaluation of the virtual performance of composite CFS joint structure as it is one of the most powerful tools to study the non-linear characteristic. Significantly, most of the previous experimental studies conducted by previous researchers are focusing more into the vigorous development of the non-composite steel structures and frames, especially for the CFS development. Conducting this study is able to provide new findings and knowledge to the composite CFS joint integrated with the normal-weight concrete slab, which is rarely investigated by previous study. New type and configurations through the isolated joint test for the proposed composite CFS joint specimens are able to provide ideas and framework to investigate in-depth of the strength and performance of the semi-rigid or partial strength of the composite CFS beam-to-column joint structure.

Proposing with new FE model with different approaches and appropriate techniques through the simulation modelling are able to simulate well the moment capacity (strength), initial rotational stiffness (stiffness) and rotational capacity (ductility). Damage for traction separation laws with “Maxps Damage” was proposed to be the best and appropriate option for the concrete preferences rather than the concrete damaged plasticity setting. Recommending to use this proposed methods and approaches of FE modelling will be able to help in exploring in-depth of the potential parameters affecting the capacity of the composite steel structure, whilst reducing the cost and time to perform the physical experimental test. Nearly accurate analysis with good strength prediction can be achieved using the numerical simulation and thus able

to provide a direct operative procedure to the construction engineers, designers and consultants involved in the composite field structure.

Supplementary Information The online version contains supplementary material available at <https://doi.org/10.1007/s13296-023-00744-0>.

Acknowledgements This work was supported by the Ministry of Higher Education under the Fundamental Research Grant Scheme (FRGS/1/2020/TKO/UTM/01/7) and Universiti Teknologi Malaysia (21H47 and 21H68).

References

- Aminuddin, K. M., Saggaff, A., & Tahir, M. M. (2017). Experimental behaviour of beam-column connection using cold-formed steel sections with rectangular gusset-plate. In: *Proceedings of the 3rd international conference on construction and building engineering (ICONBUILD) 2017* (pp. 1–7). Palembang, Indonesia. <https://doi.org/10.1063/1.5011486>
- Amsyar, F., Tan, C. S., Ma, C. K., & Sulaiman, A. (2018). Review on composite joints for cold-formed steel structures. In: *International conference on civil and environmental engineering 2018 (ICCEE 2018)* (pp. 1–11). Kuala Lumpur, Malaysia. <https://doi.org/10.1051/e3sconf/20186508006>
- Amsyar, F., Tan, C. S., Mohammad, S., Tahir, M. M., & Hamid, H. A. (2021). Partial strength beam-to-column connection of cold-formed single channel section: Numerical and experimental study. *ASM Science Journal*, 14, 1–10. <https://doi.org/10.32802/asmsej.2020.639>
- Cao, L., Li, Y., Dhanasekar, M., & Lu, C. (2021). Experimental and numerical study on flexural performance of a novel steel-encased concrete composite beam. *KSCCE Journal of Civil Engineering*, 25(5), 1837–1848. <https://doi.org/10.1007/s12205-021-1196-1>
- De Batista, E. M., & Rodrigues, F. C. (1992). Residual stress measurements on cold-formed profiles. *Experimental Techniques*, 16(5), 25–29. <https://doi.org/10.1111/j.1747-1567.1992.tb00702>
- Fahmy, A. S., Swelem, S. M., & Musstaf, H. H. (2020). Beam-column connections behavior of cold-formed steel members: New experimental configuration. *KSCCE Journal of Civil Engineering*, 24(7), 2147–2159. <https://doi.org/10.1007/s12205-020-2009-7>
- Firdaus, M., Saggaff, A., & Tahir, M. M. (2017). Finite element analysis of composite beam-to-column connection with cold-formed steel section. In: *Proceedings of the 3rd international conference on construction and building engineering (ICONBUILD) 2017* (pp. 1–8). Palembang, Indonesia. <https://doi.org/10.1063/1.5011504>
- Foraboschi, P. (2019). Lateral load-carrying capacity of steel columns with fixed-roller end supports. *Journal of Building Engineering*, 26, 1–11. <https://doi.org/10.1016/j.jobbe.2019.100879>
- Foraboschi, P. (2020). Predictive formulation for the ultimate combinations of axial force and bending moment attainable by steel members. *International Journal of Steel Structures*, 20, 705–724. <https://doi.org/10.1007/s13296-020-00316-6>
- Fu, F., Lam, D., & Ye, J. (2008). Modelling semi-rigid composite joints with precast hollowcore slabs in hogging moment region. *Journal of Constructional Steel Research*, 64, 1408–1419. <https://doi.org/10.1016/j.jcsr.2008.01.012>
- Gao, T., & Moen, C. D. (2010). The cold work of forming effect in steel structural members. In: *SDSS'Rio 2010 stability and ductility of steel structures* (pp. 1017–1024). Rio de Janeiro, Brazil.
- Hsu, C. T., Punurai, S., Punurai, W., & Majidi, Y. (2014). New composite beams having cold-formed steel joists and concrete slab.

- Engineering Structures*, 71, 187–200. <https://doi.org/10.1016/j.engstruct.2014.04.011>
- Huei, L. Y., Siang, T. C., Tahir, M., & Mohammad, S. (2012). Numerical modelling and validation of light gauge steel top-seat flange-clip connection. *Journal of Vibroengineering*, 14(3), 1104–1112.
- Kang, S. B., & Tan, K. H. (2015). Behaviour of precast concrete beam-column sub-assemblages subject to column removal. *Engineering Structures*, 93, 85–96. <https://doi.org/10.1016/j.engstruct.2015.03.027>
- Katwal, U., Zhong, T., & Hassan, M. K. (2018). Finite element modelling of steel-concrete composite beams with profiled steel sheeting. *Journal of Constructional Steel Research*, 146, 1–15. <https://doi.org/10.1016/j.jcsr.2018.03.011>
- Kim, T. S., Han, B. S., & Shin, S. W. (2007). Prediction of ultimate behavior of bolted connections in cold-formed stainless steel using numerical analysis. In: *Proceedings of the international conference on sustainable building Asia* (pp. 1093–1098). Seoul, Korea.
- Lacki, P., Nawrot, J., Derlatka, A., & Winowiecka, J. (2019). Numerical and experimental tests of steel-concrete composite beam with the connector made of top-hat profile. *Composite Structures*, 211, 244–253. <https://doi.org/10.1016/j.compstruct.2018.12.035>
- Lee, Y. H., Tan, C. S., Lee, Y. L., Tahir, M. M., Mohammad, S., & Shek, P. N. (2013). Numerical modelling of stiffness and strength behaviour of top-seat flange-clip connection for cold-formed double channel section. *Applied Mechanics and Materials*, 284–287, 1426–1430. <https://doi.org/10.4028/www.scientific.net/AMM.284-287.1426>
- Luo, Y. J., Alex, L., & Kang, Z. (2012). Parametric study of bonded steel-concrete composite beams by using finite element analysis. *Engineering Structures*, 34, 40–51. <https://doi.org/10.1016/j.engstruct.2011.08.036>
- Ozturk, A., Baran, E., & Tort, C. (2019). Nonlinear fiber modelling of steel-concrete partially composite beams with channel connectors. *KSCE Journal of Civil Engineering*, 23(5), 2227–2242. <https://doi.org/10.1007/s12205-019-1163-2>
- Prabha, P., Palani, G. S., Lakshmanan, N., & Senthil, R. (2018). Flexural behaviour of steel-foam concrete composite light-weight panels. *KSCE Journal of Civil Engineering*, 22(9), 3534–3545. <https://doi.org/10.1007/s12205-018-0827-7>
- Qiao, W., Yan, X., Zhu, R., Wang, F., & Wang, D. (2020). Flexural properties of new cold-formed thin-walled steel and concrete composite slabs. *Journal of Building Engineering*, 31, 1–13. <https://doi.org/10.1016/j.jobe.2020.101441>
- Saggaff, A., Tahir, M. M., Azimi, M., & Alhajri, T. M. (2017). Structural aspects of cold-formed steel section designed as U-shape composite beam. In: *Proceedings of the 3rd international conference on construction and building engineering (ICONBUILD) 2017* (pp. 1–11). Palembang, Indonesia. <https://doi.org/10.1063/1.5011505>
- Spoorenberg, R. C., Snijder, H. H., & Hoenderkamp, J. C. D. (2010). Experimental investigation of residual stresses in roller bent wide flange steel sections. *Journal of Constructional Steel Research*, 66(6), 737–747. <https://doi.org/10.1016/j.jcsr.2010.01.017>
- Tahir, M. M., & Siang, T. C. (2008). Experimental tests on partial strength connection for cold-formed steel of double lipped channel sections. In: *Proceedings of the 5th international conference on thin-walled structures 2008 (ICTWS 2008)* (pp. 1–8). Brisbane, Australia.
- Tan, C. S., Lee, Y. H., Lee, Y. L., Mohammad, S., Sulaiman, A., Tahir, M. M., & Shek, P. N. (2013). Numerical simulation of cold-formed steel top-seat flange clip connection. *Jurnal Teknologi*, 61(3), 63–71. <https://doi.org/10.11113/jtv61.1769>
- Weng, C. C., & Pekoz, T. (1990). Residual stresses in cold-formed steel members. *ASCE Journal of Structural Engineering*, 116(6), 1611–1625.
- Zhao, H. L., Yuan, Y., & Ye, Z. M. (2012). Simplified nonlinear simulation of steel-concrete composite beams. *Journal of Constructional Steel Research*, 71, 83–91. <https://doi.org/10.1016/j.jcsr.2011.08.015>

Publisher's Note Springer Nature remains neutral with regard to jurisdictional claims in published maps and institutional affiliations.

Springer Nature or its licensor (e.g. a society or other partner) holds exclusive rights to this article under a publishing agreement with the author(s) or other rightsholder(s); author self-archiving of the accepted manuscript version of this article is solely governed by the terms of such publishing agreement and applicable law.